IEEE Access
Multidisciplinary | Rapid Review | Open Access Journal

Received May 10, 2021, accepted May 24, 2021, date of publication May 26, 2021, date of current version June 9, 2021.

Digital Object Identifier 10.1109/ACCESS.2021.3083963

Robust Central Difference Kalman Filter With Mixture Correntropy: A Case Study for Integrated Navigation

KAIQIANG FENG[1], JIE LI[2], DEBIAO ZHANG[1], XIAOKAI WEI[1], AND JIANPING YIN[3]

[1]Key Laboratory of Instrumentation Science and Dynamic Measurement, Ministry of Education, North University of China, Taiyuan 030051, China
[2]National Key Laboratory for Electronic Measurement Technology, North University of China, Taiyuan 030051, China
[3]College of Mechatronic Engineering, North University of China, Taiyuan 030051, China

Corresponding author: Jie Li (lijie@nuc.edu.cn)

This work was supported in part by the National Natural Science Funds for Distinguished Young Scholars under Grant 51225504, in part by the National Natural Science Foundation of China under Grant 62003316 and Grant 61973280, in part by the Postdoctoral Science Foundation of China under Grant 2019M661069, and in part by the Fund for Shanxi '1331 project' Key Subject Construction.

ABSTRACT In this paper, a robust central difference Kalman filter is proposed to address the process uncertainty and non-Gaussian measurement noise induced by the vehicle's severe maneuver and abnormal measurements in MEMS-SINS/GNSS integrated navigation system. Compared with the state-of-the-art noise distribution based robust filter, in the proposed filter, the process uncertainty and measurement uncertainty are simultaneously suppressed based on a new constructed cost function, which is independent of noise distribution and more insensitive to the non-Gaussian noise. To be specific, the statistical linearization approach is first presented to derive a linear-like regression model. Then, by resorting to the innovation orthogonal theory and Cholesky triangular decomposition, the fading factor of cost function is adaptively and robustly determined in the process of iteration, where the filtering performance and the stability of the algorithm under the condition of process uncertainty are extremely enhanced. Furthermore, the correntropy using the mixture of two Gaussian functions as the kernel function is incorporated into the cost function to prevent the non-Gaussian measurement noise. Our extensive simulation and car-mounted experiment demonstrate that the proposed filter can achieve higher estimation accuracy and better robustness as compared with the related state-of-the-art methods.

INDEX TERMS MEMS-SINS/GNSS integrated navigation, robust central difference Kalman filter, mixture correntropy.

I. INTRODUCTION

MEMS-SINS/GNSS integration navigation system has been attracting significant attentions due to its widespread applications such as attitude determination and vehicle location [1]–[6]. The objective of MEMS-SINS/GNSS integration navigation is to measure the position, velocity and attitude of the carrier to satisfy the accuracy requirement. In the past few decades, Kalman filter has been the most widely used estimation strategy for the data fusion of MEMS-SINS and GNSS. One main concern of the standard Kalman filter is that they require the linear Gaussian system and depend heavily on exact prior knowledge of the system noise statistic characteristics [7]. However, these assumptions are not possible to satisfy in practical application. On one hand, the linear system does not really exist in real applications since the error model of the low-cost MEMS-SINS is essentially nonlinear [8]. On the other hand, due to the vehicle's severe maneuver and abnormal measurements in MEMS-SINS/GNSS integrated navigation system, the process uncertainty and non-Gaussian measurement noises are produced [9]–[11]. As a result, considerable estimation error or even filter divergence may be induced in the conventional KF-based MEMS-SINS/GNSS integration system. Therefore, it is necessary to design an effective filter to better solve the nonlinear and uncertainty filtering problem, which is the main focus of our work.

A large number of adaptive and robust filtering techniques have been devoted to counter the uncertain effects of the uncertainties and non-Gaussian. The adaptive

The associate editor coordinating the review of this manuscript and approving it for publication was Mauro Fadda.

filtering techniques mainly include covariance matching technique, multiple model adaptive estimation technique and covariance scaling technique. The heart of the covariance-matching method is to make the residuals consistent with their theoretical covariance [12]. However, it is hard to guarantee the estimated process and measurement noise covariance convergence to the right values. Furthermore, most covariance-matching algorithms approximate the covariance of residual using a moving window method. A large window size would provide reliable covariance measurement, but it is only suitable for the slow changing system [13]. The multiple model adaptive estimation technique handles the model uncertainty by running a bank of Kalman filters with different stochastic model simultaneously [14]. However, it is unsuitable for system with unknown dynamic since this method is under the assumption that one of the stochastic models is correct [15]. The covariance scaling technique deals with the process uncertainty by applying a scale factor to the predicted covariance to correct the predicted error covariance [16], [17]. However, it has been proven that the determination of the scale factor is unstable for the application of GNSS and MEMS-SINS integration [18]. The robust filtering techniques mainly include the Huber's M-estimation filtering technique, the student's t-based filtering technique and the particle filtering technique. Huber's M-estimation filtering solves the robust non-Gaussian filtering problem by minimizing a combined l_2 and l_2 norm [19], [20]. The residual is bounded by utilizing the robust Huber objective function. However, it is difficult to determine the true tuning factor of the Huber cost function, which may degrade the filtering performance of Huber's M-estimation filter [20]–[22]. To cope with the heavy-tailed non-Gaussian noise, many student's t-based Kalman filters have been proposed by modeling the heavy-tailed non-Gaussian measurement noise and the posterior probability density function(PDF) as student's t distribution to obtain a closed form solution [23]–[26]. However, the major disadvantage of the student's t-based Kalman filters is that they are derived under the assumption that the student's t PDFs of process and measurement noises have the same degrees of freedom(dof) parameter, which is seldom met in practical applications, resulting in a limited estimated accuracy [25]. The particle filtering deals with the non-Gaussian filtering problem by representing the required posterior density function by a set of random samples with associated weights [27]–[30]. However, the particle filter suffers from substantial computational complexity in high-dimensional problems such as MEMS-SINS/GNSS integrated navigation system since the number of the particle increase exponentially with the dimension of the state, which is not feasible for real-time implementation [31].

To address the above issues, in this paper we propose a new criterion called adaptive maximum mixture correntropy criterion(AMMCC), and develop a AMMCC–based adaptive robust filtering algorithm for MEMS-SINS/GNSS integrated navigation system dynamic state estimation. Note that in [32], [33], we have provided some preliminary results of our robust CKF to deal with both process uncertainty and non-Gaussian noise. However, the proposed RCKF is only suitable for the linear dynamic system. Additionally, the generalized maximum correntropy exhibits worse performance in strong non-Gaussian environment. This paper bridges the gap by providing the corresponding solutions. At first, the statistical linearization method is firstly used to convert the traditional nonlinear central difference Kalman filter into an equivalent linear-like regression form. Then, the criteria for bounding the state estimation error caused by process uncertainty and non-Gaussian noise is constructed. Subsequently, a new robust central difference Kalman filter based on the proposed criteria is formulated. Moreover, an adaptive strategy is proposed to automatically tune the fading factor responding to the changeable condition. Finally, simulations and car-mounted test are conducted to demonstrate the effectiveness and robustness of the proposed method. In general, our main contributions are summarized as follows:

1) The statistical linearization method is presented to convert the traditional nonlinear central difference Kalman filter into an equivalent linear-like regression form, allowing the robust estimation with maximum mixture correntropy in an efficient way.

2) A novel criterion combining the weighted least square and maximum mixture correntropy is proposed to reveal the effect of stochastic uncertainties and non-Gaussian noise on the filter design.

3) Based on the innovation orthogonal theory and Cholesky triangular decomposition, an adaptive and robust expression of the fading factor is derived in the light of the proposed RCDKF algorithm, yielding a better filtering performance against time-varing process noise.

The remainder of this paper is organized as follows. Section II briefly reviews the maximum correntropy criterion and the main structure of central difference Kalman filter. In section III, the proposed robust central difference Kalman filter approach is introduced in detail. In section IV, simulations and experiments for the MEMS-SINS/GNSS integration navigation system are studied to demonstrate the effectiveness of the proposed method. Finally, conclusions are drawn in section V.

II. PRELIMINARIES

A. MIXTURE CORRENTROPY

Correntropy is a local similarity measure between two random variables defined in kernel space [34]–[36]. Given two scalar random variables X and Y, their correntropy is defined by:

$$V(X, \mathrm{Y}) = E[\kappa(X, \mathrm{Y})] = \int \kappa(x, y)\, dF_{XY}(x, y) \quad (1)$$

where $E[\cdot]$ denotes the expectation operator, $F_{XY}(x, y)$ is the joint probability density function of X and Y, κ (x, y) is the Mercer's type positive definite kernel function. Generally, the Gaussian kernel function is selected as the most widely

used kernel in correntropy, which is given by:

$$\kappa\left(\mathrm{x}, y\right)=G_{\sigma}\left(x-y\right)=\exp\left(-\frac{\|x-y\|^{2}}{2\sigma^{2}}\right) \tag{2}$$

where $\sigma > 0$ denotes the kernel bandwidth of correntropy. Given N samples $\{x_i, y_i\}_{i=1}^{N}$ of the random variables X and Y, the correntropy between X and Y is always estimated by using the sample estimator with N data points as follow:

$$\hat{V}\left(X, \mathrm{Y}\right)=\frac{1}{N}\sum_{i=1}^{N}G_{\sigma}\left(x_i-y_i\right) \tag{3}$$

The properties of correntropy and the advantages of its associated maximum correntropy criterion can be referred to [37]–[39]. However, it should be noted that the correntropy is sensitive to the Gaussian kernel bandwidth, resulting in a single kernel parameter may suffer performance degradation in the traditional maximum correntropy criterion based Kalman filter. Hence, to further improve the robust performance, in this paper we introduce the concept of mixture correntropy, which uses the mixture of two Gaussian functions as the kernel function, i.e.,

$$M\left(X, Y\right)=E\left[\alpha G_{\sigma_1}\left(e\right)+\left(1-\alpha\right)G_{\sigma_2}\left(e\right)\right] \tag{4}$$

where σ_1 and σ_2 are respectively the kernel bandwidths of the Gaussian kernel functions $G_{\sigma_1}(\cdot)$ and $G_{\sigma_2}(\cdot)$, $0 \le \alpha \le 1$ is the mixture coefficient. It should be noted that the mixture correntropy will reduce to the correntropy with single kernel function. In addition, it has been proven that the mixture correntropy with a proper coefficient can outperform the original correntropy in robust filtering.

B. CENTRAL DIFFERENCE KALMAN FILTER

The central difference Kalman filter can achieve the most high estimation accuracy among all the sigma-point Kalman filters by using sterling interpolation formula. Therefore, the central difference Kalman filter is chosen as the representation of the nonlinear filtering methods to address the state estimation of integration navigation system in this paper. Consider the non-linear discrete-time dynamic system with addictive noise as follows:

$$\begin{cases}\mathbf{x}_k=f\left(\mathbf{x}_{k-1}\right)+\mathbf{w}_{k-1}\\ \mathbf{z}_k=h\left(\mathbf{x}_k\right)+\mathbf{v}_k\end{cases} \tag{5}$$

where k is the discrete time index, $\mathbf{x}_k \in \mathbb{R}^{n\times 1}$ is the n-dimensional system state at time step k, $\mathbf{z}_k \in \mathbb{R}^{n\times 1}$ is the m-dimensional measurement vector at discrete time k; $f(\cdot)$ and $h(\cdot)$ are respectively the nonlinear dynamic model and measurement model. $\mathbf{w}_{k-1}$ and $\mathbf{v}_k$ are assumed to be process and measurement Gaussian noise sequences with zero means and variances $\mathbf{Q}_{k-1}$ and $\mathbf{R}_{k-1}$, respectively.

Generally, the central difference Kalman filter mainly contains the following three steps: initialization, prediction and update.

1) INITIALIZATION

$$\begin{aligned}\hat{\mathbf{x}}_0&=E\left[\mathbf{x}_0\right]\\ \mathbf{P}_{x_0}&=E\left[\left(\mathbf{x}_0-\hat{\mathbf{x}}_0\right)\left(\mathbf{x}_0-\hat{\mathbf{x}}_0\right)^{T}\right]\end{aligned} \tag{6}$$

2) PREDICTION

For $k = 2, \cdots \infty$

(1) Calculate the sigma-points for time-update:

$$\boldsymbol{\chi}_{k-1}=\left[\hat{x}_{k-1}, \hat{x}_{k-1}+h\sqrt{\mathbf{P}_{x_{k-1}}}, \hat{x}_{k-1}-h\sqrt{\mathbf{P}_{x_{k-1}}}\right] \tag{7}$$

(2) Evaluate the propagated sigma-points through the state equation:

$$\mathbf{X}^{*}_{i,k|k-1}=f\left(\boldsymbol{\chi}_{i,k-1}\right),\quad i=1,2,3\ldots 2n+1 \tag{8}$$

(3)Determine the weights:

$$w_i^{(m)}=\begin{cases}\left(h^2-n\right)/h^2, & i=1\\ 1/2h^2, & i=2,\cdots,2n+1\end{cases} \tag{9}$$

$$w_i^{(c_1)}=\frac{1}{4h^2},\ w_i^{(c_2)}=\frac{h^2-1}{4h^4}\ (i=2,\cdots,2n+1) \tag{10}$$

where h is the scalar central difference step size. Generally, $h=\sqrt{3}$ is optimally selected.

(4) Estimate the prior state and evaluate the corresponding error covariance matrix

$$\hat{\mathbf{x}}_{k|k-1}=\sum_{i=1}^{2n+1}\omega_i^{m}\mathbf{X}^{*}_{i,k|k-1} \tag{11}$$

$$\begin{aligned}\mathbf{P}_{k|k-1}=&\sum_{i=1}^{n}\left[w_i^{c1}\left(\mathbf{X}^{*}_{i,k|k-1}-\mathbf{X}^{*}_{i+n,k|k-1}\right)^{2}\right.\\ &\left.+w_i^{c2}\left(\mathbf{X}^{*}_{i,k|k-1}+\mathbf{X}^{*}_{i+n,k|k-1}-2\mathbf{X}^{*}_{0,k|k-1}\right)^{2}\right]\\ &+\mathbf{Q}_{k-1}\end{aligned} \tag{12}$$

Update:

(1) Update the sigma-points for measurement-update:

$$\boldsymbol{\chi}_{k|k-1}=\left[\hat{x}_{k|k-1}, \hat{x}_{k|k-1}+h\sqrt{\mathbf{P}_{x_{k|k-1}}}, \hat{x}_{k|k-1}-h\sqrt{\mathbf{P}_{x_{k|k-1}}}\right] \tag{13}$$

(2) Evaluate the propagated sigma-points through the measurement equation

$$\mathbf{Z}_{i,k|k-1}=h\left(\boldsymbol{\chi}_{i,k|k-1}\right) \tag{14}$$

(3) Estimate the priori measurement

$$\hat{\mathbf{z}}_{k|k-1}=\sum_{i=1}^{2n+1}\omega_i^{m}\mathbf{Z}_{i,k|k-1} \tag{15}$$

(4) Estimate the covariance matrix, cross covariance matrix and compute the Kalman gain

$$\begin{aligned}\mathbf{P}_{zz,k|k-1}=&\sum_{i=1}^{n}\left[w_i^{c1}\left(\mathbf{Z}^{*}_{i,k|k-1}-\mathbf{Z}^{*}_{i+n,k|k-1}\right)^{2}\right.\\ &\left.+w_i^{c2}\left(\mathbf{Z}^{*}_{i,k|k-1}+\mathbf{Z}^{*}_{i+n,k|k-1}-2\mathbf{Z}^{*}_{0,k|k-1}\right)^{2}\right]\\ &+\mathbf{R}_k\end{aligned} \tag{16}$$

$$\mathbf{P}_{xz,k|k-1} = \sqrt{w_i^{c1} P_{k|k-1}} \left[\mathbf{Z}_{1:n,k|k-1} - \mathbf{Z}_{n+1:2n,k|k-1}\right] \quad (17)$$

$$\mathbf{K}_k = \mathbf{P}_{xz,k|k-1} / \mathbf{P}_{zz,k|k-1} \quad (18)$$

(5) Estimate the posterior state and the corresponding error covariance matrix

$$\hat{\mathbf{x}}_{k|k} = \hat{\mathbf{x}}_{k|k-1} + \mathbf{K}_k \left(\mathbf{z}_k - \hat{\mathbf{z}}_{k|k-1}\right) \quad (19)$$

$$\mathbf{P}_{k|k} = \mathbf{P}_{k|k-1} - \mathbf{K}_k \mathbf{P}_{zz,k|k-1} \mathbf{K}_k^T \quad (20)$$

III. THE PROPOSED ROBUST CENTRAL DIFFERENCE KALMAN FILTER

In this section, the statistical linearization method is firstly used to convert the traditional nonlinear central difference Kalman filter into an equivalent linear-like regression form. Then, the criteria for bounding the state estimation error caused by process uncertainty and non-Gaussian noise is constructed. Finally, by utilizing the criteria, the main steps to develop the new robust central difference Kalman filter are presented in detail.

A. DERIVATION OF THE LINEAR-LIKE REGRESSION FORM OF THE CENTRAL DIFFERENCE KALMAN FILTER

Consider the nonlinear measurement equation in (5), we apply a statistic linearization around $\hat{\mathbf{x}}_{k|k-1}$ yielding:

$$\mathbf{z}_k = \hat{\mathbf{z}}_{k|k-1} + \tilde{\mathbf{H}}_k \left(\hat{\mathbf{x}}_k - \hat{\mathbf{x}}_{k|k-1}\right) + \boldsymbol{\eta}_k + \mathbf{v}_k \quad (21)$$

where $\tilde{\mathbf{H}}_k = \left(\mathbf{P}_{xz,k|k-1}\right)^T \mathbf{P}_{k|k-1}^{-1}$ is the measurement slope matrix, $\boldsymbol{\eta}_k$ is the statistical linearization error term which is used to compensate the high order Taylor-series expansion error. The covariance matrix of $\boldsymbol{\eta}_k$ is calculated as:

$$\hat{\mathbf{R}}_k = E\left[\boldsymbol{\eta}_k \boldsymbol{\eta}_k^T\right] = \mathbf{P}_{zz,k|k-1} - \left(\mathbf{P}_{xz,k|k-1}\right)^T \mathbf{P}_{k|k-1}^{-1} \mathbf{P}_{xz,k|k-1} \quad (22)$$

Then the linear regression form of (21) can be constructed as follows:

$$\tilde{\mathbf{z}}_k = \tilde{\mathbf{H}}_k \mathbf{x}_k + \xi_k \quad (23)$$

where $\tilde{\mathbf{z}}_k = \mathbf{z}_k - \hat{\mathbf{z}}_{k|k-1} + \tilde{\mathbf{H}}_k \hat{\mathbf{x}}_{k|k-1}$, $\xi_k = \boldsymbol{\eta}_k + \mathbf{v}_k$, the corresponding error covariance matrix $\mathbf{W}_k$ is obtained as:

$$\mathbf{W}_k = E\left[\xi_k \xi_k^T\right] = \sum\nolimits_k = \mathbf{B}_k \mathbf{B}_k^T \quad (24)$$

where $\sum_k = E\left[\left(\boldsymbol{\eta}_k + \mathbf{v}_k\right)\left(\boldsymbol{\eta}_k + \mathbf{v}_k\right)^T\right] = \mathbf{R}_k + \hat{\mathbf{R}}_k$, $\mathbf{B}_k$ can be obtained by the Cholesky decomposition of $\mathbf{W}_k$. Left multiplying both sides of (23) by $\mathbf{B}_k^{-1}$, the statistical linear regression model can be transformed to

$$\mathbf{D}_k = g\left(\mathbf{x}_k\right) + \boldsymbol{\xi}_k \quad (25)$$

where $\mathbf{D}_k = \mathbf{B}_k^{-1} \tilde{\mathbf{z}}_k$, $g\left(\mathbf{x}_k\right) = \mathbf{B}_k^{-1} \tilde{\mathbf{H}}_k \mathbf{x}_k$ and $\boldsymbol{\varepsilon}_k = \mathbf{B}_k^{-1} \boldsymbol{\xi}_k$.

B. CRITERIA FOR PROCESS UNCERTAINTY AND NON-GAUSSIAN NOISE

The process uncertainty and non-Gaussian noise inevitably degrade the performance of the traditional central difference Kalman filter significantly. In order to solve the problem, motivated by the cost function of weighted least square (WLS), we propose in this work to use the residual orthogonal principle based WLS method to deal with process uncertainty and the mixture correntropy to handle the non-Gaussian measurement noise, and then establish the new criteria named AMMCC as follows:

$$J_L\left(x_k\right) = \left\|\mathbf{x}_k - \hat{\mathbf{x}}_{k|k-1}\right\|^2_{\left(\boldsymbol{\lambda}_k \mathbf{p}_{k|k-1}\right)^{-1}} + \sum_{i=1}^{m} \rho_{MIX-CC}\left(\mathbf{e}_{k,i}\right) \quad (26)$$

where $\|x\|_A^2 = x^T A x$ is the quadratic form with respect to A. $\hat{\mathbf{x}}_{k|k-1}$ denotes the prediction of state $\mathbf{x}_k$ at time step k, and $\mathbf{P}_{k|k-1}$ denote the corresponding error covariance. λ_k is the fading factor, which is used to strengthen the robustness of the proposed filter against the process uncertainty. $\rho_{MIX-CC}\left(\mathbf{e}_{k,i}\right) = \left(1 - \alpha \frac{\exp\left(-e_{k,i}^2/2\sigma_1^2\right)}{\sqrt{2\pi}\sigma_1} - (1-\alpha) \frac{\exp\left(-e_{k,i}^2/2\sigma_2^2\right)}{\sqrt{2\pi}\sigma_2}\right)$, $\mathbf{e}_{k,i} = \mathbf{D}_{k,i} - g\left(\mathbf{x}_{k,i}\right)$, $\mathbf{e}_{k,i}$ is the i-th element of $\mathbf{e}_k$, and m is the dimension of $\mathbf{D}_k$.

Then, under the new cost function defined above, the linear regress problem in (25) can be solved robustly by minimizing the following function:

$$\hat{\mathbf{x}}_k = \arg\min_{\mathbf{x}_k} \left(\left\|\mathbf{x}_k - \hat{\mathbf{x}}_{k|k-1}\right\|^2_{\left(\boldsymbol{\lambda}_k \mathbf{p}_{k|k-1}\right)^{-1}} + \sum_{i=1}^{m} \rho_{MIX-CC}\left(\mathbf{e}_{k,i}\right) \right) \quad (27)$$

C. ROBUST CENTRAL DIFFERENCE KALMAN FILTER

In order to suppress the adverse effects of process uncertainty and non-Gaussian noise, in this part, a robust central difference Kalman filter (RCDKF) is designed based on the aforementioned criterion.

The optimal solution of (27) can be found by differencing the cost function with respected to $\mathbf{x}_k$ as:

$$\left(\boldsymbol{\lambda}_k \mathbf{P}_{k|k-1}\right)^{-1} \left(\mathbf{x}_k - \hat{\mathbf{x}}_{k|k-1}\right) - \sum_{i=1}^{m} \left(\alpha \psi_1\left(\mathbf{e}_{k,i}\right) \frac{\partial \mathbf{e}_{k,i}}{\partial \mathbf{x}_k} + (1-\alpha)\, \psi_2\left(\mathbf{e}_{k,i}\right) \frac{\partial \mathbf{e}_{k,i}}{\partial \mathbf{x}_k} \right) = 0 \quad (28)$$

where $\psi_1\left(\mathbf{e}_{k,i}\right) = -\frac{\mathrm{G}_{\sigma_1}\left(\mathbf{e}_{k,i}\right) \cdot \mathbf{e}_{k,i}}{\sigma_1^2}$, $\psi_2\left(\mathbf{e}_{k,i}\right) = -\frac{\mathrm{G}_{\sigma_2}\left(\mathbf{e}_{k,i}\right) \cdot \mathbf{e}_{k,i}}{\sigma_2^2}$, thus we can simplify equation (28) as follows:

$$\left(\boldsymbol{\lambda}_k \mathbf{P}_{k|k-1}\right)^{-1} \left(\mathbf{x}_k - \hat{\mathbf{x}}_{k|k-1}\right) + \sum_{i=1}^{m} \left(\alpha \frac{\mathrm{G}_{\sigma_1}\left(\mathbf{e}_{k,i}\right)}{\sigma_1^2} + (1-\alpha) \frac{\mathrm{G}_{\sigma_2}\left(\mathbf{e}_{k,i}\right)}{\sigma_2^2} \right) \mathbf{e}_{k,i} \frac{\partial \mathbf{e}_{k,i}}{\partial \mathbf{x}_k} = 0 \quad (29)$$

Defining the function $\mathbf{C}_{k,i} = \alpha \frac{\mathrm{G}_{\sigma_1}(\mathbf{e}_{k,i})}{\sigma_1^2} + (1-\alpha)\frac{\mathrm{G}_{\sigma_2}(\mathbf{e}_{k,i})}{\sigma_2^2}$ and dialog matrix $\mathbf{C_k} = diag\left[\mathbf{C}_{k,i}\right] i = 1, \cdots, \mathrm{m}$, we can rewrite equation (29) as follows:

$$\left(\boldsymbol{\lambda}_k \mathbf{P}_{k|k-1}\right)^{-1}\left(\mathbf{x}_k - \hat{\mathbf{x}}_{k|k-1}\right) + \mathbf{C_k}\mathbf{e}_k \frac{\partial \mathbf{e}_k}{\partial \mathbf{x}_k} = 0 \tag{30}$$

Substituting $\mathbf{e}_k = \mathbf{D}_k - g\left(\mathbf{x}_k\right) = \mathbf{B}_k^{-1}\left(\tilde{\mathbf{z}}_k - \tilde{\mathbf{H}}_k \mathbf{x}_k\right)$ into (30), it can be obtained as follows:

$$\begin{aligned}\left(\boldsymbol{\lambda}_k \mathbf{P}_{k|k-1}\right)^{-1}&\left(\mathbf{x}_k - \hat{\mathbf{x}}_{k|k-1}\right)\\ &-\mathbf{H}_k^T \mathbf{B}_k^{-T}\mathbf{C}_k \mathbf{B}_k^{-1}\left(\tilde{\mathbf{z}}_k - \tilde{\mathbf{H}}_k \mathbf{x}_k\right) = 0\end{aligned} \tag{31}$$

Let $\bar{\mathbf{P}}_{k|k-1} = \lambda_k \mathbf{P}_{k|k-1}$, $\bar{\mathbf{R}}_k = \mathbf{B}_k \mathbf{C}_k^{-1} \mathbf{B}_k^T$ and $\hat{\mathbf{x}}_{k|k} = \mathbf{x}_k$, we have:

$$\bar{\mathbf{P}}_{k|k-1}^{-1}\left(\hat{\mathbf{x}}_{k|k} - \hat{\mathbf{x}}_{k|k-1}\right) = \mathbf{H}_k^T \bar{\mathbf{R}}_k^{-1}\left(\tilde{\mathbf{z}}_k - \tilde{\mathbf{H}}_k \hat{\mathbf{x}}_{k|k}\right) \tag{32}$$

Equation (32) can be organized as follows:

$$\begin{aligned}&\left(\bar{\mathbf{P}}_{k|k-1}^{-1} + \tilde{\mathbf{H}}_k^T \bar{\mathbf{R}}_k^{-1}\tilde{\mathbf{H}}_k\right)\hat{\mathbf{x}}_{k|k}\\ &= \bar{\mathbf{P}}_{k|k-1}^{-1}\hat{\mathbf{x}}_{k|k-1} + \tilde{\mathbf{H}}_k^T \bar{\mathbf{R}}_k^{-1}\mathbf{z}_k\\ &\quad -\tilde{\mathbf{H}}_k^T \bar{\mathbf{R}}_k^{-1}\tilde{\mathbf{H}}_k \hat{\mathbf{x}}_{k|k-1} + \tilde{\mathbf{H}}_k^T \bar{\mathbf{R}}_k^{-1}\tilde{\mathbf{H}}_k \hat{\mathbf{x}}_{k|k-1}\end{aligned} \tag{33}$$

$$\begin{aligned}&\left(\bar{\mathbf{P}}_{k|k-1}^{-1} + \tilde{\mathbf{H}}_k^T \bar{\mathbf{R}}_k^{-1}\tilde{\mathbf{H}}_k\right)\hat{\mathbf{x}}_{k|k}\\ &= \left(\bar{\mathbf{P}}_{k|k-1}^{-1} + \tilde{\mathbf{H}}_k^T \bar{\mathbf{R}}_k^{-1}\tilde{\mathbf{H}}_k\right)\hat{\mathbf{x}}_{k|k-1}\\ &\quad +\tilde{\mathbf{H}}_k^T \bar{\mathbf{R}}_k^{-1}\left(\tilde{\mathbf{z}}_k - \tilde{\mathbf{H}}_k \hat{\mathbf{x}}_{k|k-1}\right)\end{aligned} \tag{34}$$

Left multiplying both sides of (34) by $\left(\bar{\mathbf{P}}_{k|k-1}^{-1} + \tilde{\mathbf{H}}_k^T \bar{\mathbf{R}}_k^{-1}\tilde{\mathbf{H}}_k\right)^{-1}$, it can be obtained as follows:

$$\begin{aligned}\hat{\mathbf{x}}_{k|k} &= \hat{\mathbf{x}}_{k|k-1} + \mathbf{K}_k\left(\tilde{\mathbf{z}}_k - \tilde{\mathbf{H}}_k \hat{\mathbf{x}}_{k|k-1}\right)\\ &= \hat{\mathbf{x}}_{k|k-1} + \mathbf{K}_k\left(\mathbf{z}_k - \tilde{\mathbf{z}}_{k|k-1}\right)\end{aligned} \tag{35}$$

$$\mathbf{K}_k = \left(\bar{\mathbf{P}}_{k|k-1}^{-1} + \tilde{\mathbf{H}}_k^T \bar{\mathbf{R}}_k^{-1}\tilde{\mathbf{H}}_k\right)^{-1}\tilde{\mathbf{H}}_k^T \bar{\mathbf{R}}_k^{-1} \tag{36}$$

Meanwhile, the corresponding posterior covariance matrix can be updated by:

$$\begin{aligned}\bar{\mathbf{P}}_{k|k} &= \left(\mathrm{I} - \mathbf{K}_k \tilde{\mathbf{H}}_k\right)\bar{\mathbf{P}}_{k|k-1}\left(\mathrm{I} - \mathbf{K}_k \tilde{\mathbf{H}}_k\right)^T + \mathbf{K}_k \bar{\mathbf{R}}_k \mathbf{K}_k^T\\ &= \left(\mathrm{I} - \mathbf{K}_k \tilde{\mathbf{H}}_k\right)\bar{\mathbf{P}}_{k|k-1}\end{aligned} \tag{37}$$

Remark 1: It should be noted that the proposed RCDKF has a similar structure as that of the traditional Kalman filter. In the proposed RCDKF, we use the weighted least square and robust statistical linearization regression based maximum mixture correntropy to obtain the prior and posterior estimates of the state and covariance matrix. Taking advantage of AMMCC, the proposed RCDKF can extensively increase the robustness to the process uncertainty and non-Gaussian noise at a lower computation cost with acceptable estimation performance as compared with the existing noise distribution based robust filtering algorithms.

D. PARAMETER DETERMINATION OF THE PROPOSED RCDKF

For practical integration navigation system, the process covariance matrix is heavily depending on the actual operating conditions of the system and changing from time to time. Therefore, in order to further enhance the robustness of the proposed method and accommodate the changeable noise environment, the fading factor $\boldsymbol{\lambda}_k$ for the one-step prediction error covariance matrix should be estimated dynamically at each time instant.

As we all know, the residual sequence should remain orthogonal at different times for the proposed RCDKF. Thereby, the fading factor $\boldsymbol{\lambda}_k$ can be determined by solving the following optimization problem:

$$E\left(\left[x_k - \hat{x}_k\right]\left[x_k - \hat{x}_k\right]^T\right) = \min \tag{38}$$

$$E\left(\varepsilon_k \varepsilon_{k+j}^T\right) = \min \quad j = 1, 2..... \tag{39}$$

The sufficient condition of $E\left[\boldsymbol{\varepsilon}_{k+j}\boldsymbol{\varepsilon}_k^T\right] = 0$ is as follows:

$$\bar{\mathbf{P}}_{k|k-1}\tilde{\mathbf{H}}_k^T - \mathbf{K}_k \mathbf{V}_k \equiv 0 \tag{40}$$

where $\mathbf{V}_k = \left(\tilde{\mathbf{z}}_k - \tilde{\mathbf{H}}_k \mathbf{x}_{k|k-1}\right)\left(\tilde{\mathbf{z}}_k - \tilde{\mathbf{H}}_k \mathbf{x}_{k|k-1}\right)^T$ denotes the residual error sequence covariance matrix. Substituting (36) into (40), it can be obtained as follows:

$$\bar{\mathbf{P}}_{k|k-1}\tilde{\mathbf{H}}_k^T - \bar{\mathbf{P}}_{k|k-1}\tilde{\mathbf{H}}_k^T\left(\tilde{\mathbf{H}}_k \bar{\mathbf{P}}_{k|k-1}\tilde{\mathbf{H}}_k^T + \mathbf{R}_k\right)^{-1}\mathbf{V}_k \equiv 0 \tag{41}$$

The sufficient condition for the establishment of (41) is as follows:

$$\tilde{\mathbf{H}}_k \bar{\mathbf{P}}_{k|k-1}\tilde{\mathbf{H}}_k^T = \mathbf{V}_k - \mathbf{R}_k \tag{42}$$

Substituting $\bar{\mathbf{P}}_{k|k-1} = \boldsymbol{\lambda}_k \mathbf{P}_{k|k-1}$ into (42), it can be obtained as follows:

$$\tilde{\mathbf{H}}_k\left(\lambda_k \mathbf{P}_{k|k-1}\right)\tilde{\mathbf{H}}_k^T = \mathbf{V}_k - \mathbf{R}_k \tag{43}$$

Substituting (12) into (43), it can be organized as follows:

$$\tilde{\mathbf{H}}_k\left(\lambda_k \mathbf{P}_{k-1}\right)\tilde{\mathbf{H}}_k^T = \mathbf{V}_k - \mathbf{R}_k - \tilde{\mathbf{H}}_k \mathbf{Q}_{k-1}\tilde{\mathbf{H}}_k^T \tag{44}$$

where

$$\begin{aligned}\mathbf{P}_{k-1} = \sum_{i=1}^{n}\Bigg[&w_i^{c1}\left(\mathbf{X}_{i,k|k-1}^* - \mathbf{X}_{i+n,k|k-1}^*\right)^2\\ &+ w_i^{c2}\left(\mathbf{X}_{i,k|k-1}^* + \mathbf{X}_{i+n,k|k-1}^* - 2\mathbf{X}_{0,k|k-1}^*\right)^2\Bigg].\end{aligned}$$

In order to make different date channel have different fading rate, the multiple fading factor is used to change the working way of single fading factor matrix, thus the equation (44) can be rewritten as follows:

$$\tilde{\mathbf{H}}_k\left(\Delta_k \mathbf{P}_{k-1}\Delta_k^T\right)\tilde{\mathbf{H}}_k^T = \mathbf{V}_k - \mathbf{R}_k - \tilde{\mathbf{H}}_k \mathbf{Q}_{k-1}\tilde{\mathbf{H}}_k^T \tag{45}$$

where Δ_k is obtained by the Cholesky decomposition as follows:

$$\lambda_k = \Delta_k \Delta_k^T \tag{46}$$

where $\Delta_k = diag\left\{\sqrt{\lambda_k^1}, \sqrt{\lambda_k^2}, \cdots \sqrt{\lambda_k^n}\right\}\sigma_k$, $\sigma_k = diag\{\sigma_{11}, \sigma_{22}, \cdots \sigma_{nn}\}$ is a constant coefficients aiming at each state variable predetermined by priori information.

Calculating the trace on both sides of (45), we can obtain

$$tr\left[\tilde{\mathbf{H}}_k\left(\Delta_k \mathbf{P}_{k-1}\Delta_k^T\right)\tilde{\mathbf{H}}_k^T\right] = tr\left[\mathbf{V}_k - \mathbf{R}_k - \tilde{\mathbf{H}}_k\mathbf{Q}_{k-1}\tilde{\mathbf{H}}_k^T\right] \tag{47}$$

According to the property of matrix trace $tr[\mathbf{M}_1\mathbf{M}_2] = tr[\mathbf{M}_2\mathbf{M}_1]$, equation (47) can be organized as follows:

$$tr\left[\left(\Delta_k \mathbf{P}_{k-1}\Delta_k^T\right)\tilde{\mathbf{H}}_k^T\tilde{\mathbf{H}}_k\right] = tr\left[\mathbf{V}_k - \mathbf{R}_k - \tilde{\mathbf{H}}_k\mathbf{Q}_{k-1}\tilde{\mathbf{H}}_k^T\right] \tag{48}$$

Considering that the fading factor should be greater than 1, thus the multiple fading factor can be obtained as follows:

$$\Delta_k = \max\left(1, \sqrt{\frac{tr\,(N_k)}{tr\,(M_k)}}\sigma_k\right) \tag{49}$$

$$N_k = \mathbf{V}_k - \mathbf{R}_k - \tilde{\mathbf{H}}_k\mathbf{Q}_{k-1}\tilde{\mathbf{H}}_k^T \tag{50}$$

$$M_k = \left(\sigma_k \mathbf{P}_{k-1}\sigma_k^T\right)\tilde{\mathbf{H}}_k^T\tilde{\mathbf{H}}_k \tag{51}$$

Remark 2: Based on the innovation orthogonal theory, a novel adaptive fading factor is designed. As compared with the existing fading factor, the main advantage is that the Cholesky triangular decomposition is used to avoid the destruction of symmetry and divergence introduced by λ_k. By employing the proposed fading factor, the covariance matrices of process noise can be adjust dynamically with the actual working conditions of the integrated navigation system, which further enhance the robustness and stability of the proposed method, and a much better estimation performance can be achieved.

E. SUMMARY OF THE PROPOSED ALGORITHM

The implementation pseudocode for the proposed RCDKF algorithm is presented as Alogrithm 1. The implementation procedure of the proposed RCDKF is displayed in Figure 1.

IV. PERFORMANCE EVALUATION AND ANALYSIS

In order to evaluate the performance of the proposed RCDKF, this section will provide the quantitative performance in detail by simulations and car-mounted field tests for MEMS-SINS/GNSS integrated navigation.

A. FILTERING MODEL OF MEMS-SINS/GNSS

The SINS body frame is denoted by b-frame (Front-Up-Right), the local level navigation frame is denoted by n-frame (North-Up-East), the earth frame is denoted by e-frame, and the inertial frame is denoted by i-frame. The state vector for the low-cost tightly coupled MEMS-SINS/GNSS is selected as:

$$\mathbf{x} = \left[\boldsymbol{\phi}^n\ \delta\mathbf{v}^n\ \delta\mathbf{p}^n\ \mathbf{b}_g\ \mathbf{b}_f\delta\ \mathbf{b}_g\ \delta\mathbf{b}_f\ \delta\mathbf{b}_r\ \delta\mathbf{d}_r\right]^T \tag{52}$$

where $\boldsymbol{\psi}^n$, $\delta\mathbf{v}^n$, $\delta\mathbf{p}^n$ are respectively the attitude error, velocity error and position error expressed in the n-frame. $\mathbf{b}_g$ and $\mathbf{b}_f$ represent the static biases of tri-axis gyroscope and accelerometer resolving in the b-frame, respectively. $\delta\mathbf{b}_g$ and

Algorithm 1 One Time Step of the Proposed RCDKF

Initialization: $\hat{\mathbf{x}}_{0|0}$, $\bar{\mathbf{P}}_{0|0}$, σ_1, σ_2

Time Update:

1. Compute the predicted state vector $\hat{\mathbf{x}}_{k|k-1}$ and the corresponding error covariance matrix $\mathbf{P}_{k|k-1}$ using (7) - (12);
2. Calculate $\mathbf{B}_k$ by applying Cholesky decomposition $\mathbf{R}_k = \mathbf{B}_k\mathbf{B}_k^T$;
3. Calculate $\mathbf{e}_{k,i}$ using $\mathbf{e}_{k,i} = \mathbf{D}_{k,i} - g\left(\mathbf{x}_{k,i}\right)$, where $\mathbf{D}_k = \mathbf{B}_k^{-1}\tilde{\mathbf{z}}_k$, $g\left(\mathbf{x}_k\right) = \mathbf{B}_k^{-1}\tilde{\mathbf{H}}_k\mathbf{x}_k$;
4. Calculate $\mathbf{C}_k$ using $\mathbf{C}_k = diag\left[\mathbf{C}_{k,i}\right] i = 1, \cdots, m$, where $\mathbf{C}_{k,i} = \alpha\frac{G_{\sigma_1}(\mathbf{e}_{k,i})}{\sigma_1^2} + (1-\alpha)\frac{G_{\sigma_2}(\mathbf{e}_{k,i})}{\sigma_2^2}$
5. Calculate $\bar{\mathbf{R}}_k$ using $\bar{\mathbf{R}}_k = \mathbf{B}_k\mathbf{C}_k^{-1}\mathbf{B}_k^T$;
6. Calculate the multiple fading factor Δ_k using (49)-(51);
7. $\bar{\mathbf{P}}_{k|k-1} = \Delta_k\mathbf{P}_{k|k-1}\Delta_k^T$

Measurement Update:

8. $\mathbf{K}_k = \frac{\bar{\mathbf{P}}_{k|k-1}\tilde{\mathbf{H}}_k^T}{\bar{\mathbf{R}}_k + \tilde{\mathbf{H}}_k\bar{\mathbf{P}}_{k|k-1}\tilde{\mathbf{H}}_k^T}$

$\hat{\mathbf{x}}_{k|k} = \hat{\mathbf{x}}_{k|k-1} + \mathbf{K}_k\left(\tilde{\mathbf{z}}_k - \tilde{\mathbf{H}}_k\hat{\mathbf{x}}_{k|k-1}\right)$

$\bar{\mathbf{P}}_{k|k} = \left(\mathbf{I} - \mathbf{K}_k\tilde{\mathbf{H}}_k\right)\bar{\mathbf{P}}_{k|k-1}\left(\mathbf{I} - \mathbf{K}_k\tilde{\mathbf{H}}_k\right)^T + \mathbf{K}_k\bar{\mathbf{R}}_k\mathbf{K}_k^T$
$= \left(\mathbf{I} - \mathbf{K}_k\tilde{\mathbf{H}}_k\right)\bar{\mathbf{P}}_{k|k-1}$

Output: $\hat{\mathbf{x}}_{k|k}$, $\bar{\mathbf{P}}_{k|k}$

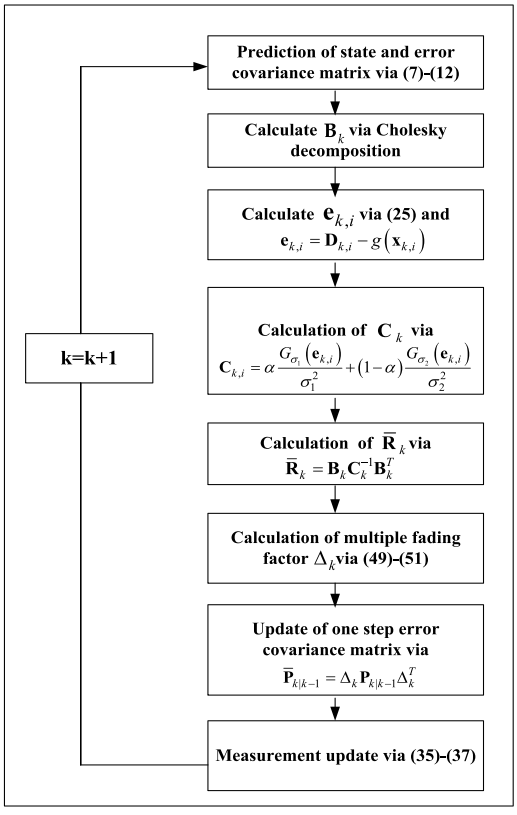

FIGURE 1. The implementation procedure of RCDKF.

$\delta\mathbf{b}_f$ are respectively the dynamic biases of tri-axis gyroscope and accelerometer expressed in the b-frame. The nonlinear system error equation of SINS can be formulated as:

$$\begin{cases} \dot{\varphi}^n = \mathbf{C}_w \left[\left(\mathrm{I} - \mathbf{C}_n^p \right) w_{in}^n + \delta w_{in}^n - \mathbf{C}_b^p \delta w_{ib}^b \right] \\ \delta \dot{\mathbf{v}}^n = \left(\mathrm{I} - \mathbf{C}_p^n \right) \mathbf{C}_b^p f_{ib}^b + \mathbf{C}_b^p \delta f_{ib}^b + \delta \mathbf{v}^n \\ \qquad \times \left(2 w_{ie}^n + w_{en}^n \right) + \mathbf{v}^n \times \left(2 \delta w_{ie}^n + \delta w_{en}^n \right) \\ \delta \dot{\lambda} = \dfrac{\delta V_E}{R_N + h} \sec L + \delta L \dfrac{V_E \sec L}{R_N + h} \tan L \\ \delta \dot{L} = \dfrac{\delta V_N}{R_N + h} \\ \delta \dot{h} = \delta V_U \\ \dot{b}_g = 0 \\ \dot{b}_f = 0 \\ \delta \dot{b}_g = -\dfrac{1}{\tau_g} \delta b_g + \eta_g \\ \delta \dot{b}_f = -\dfrac{1}{\tau_f} \delta b_f + \eta_f \end{cases} \tag{53}$$

where $\mathbf{C}_w$ denotes the transformation matrix from angle rate to Euler angle, $\mathbf{C}_n^p$ the attitude rotation matrix from n-frame(ideal navigation frame) to p-frame(actual navigation frame), $\mathbf{C}_b^p$ the attitude rotation matrix from the body frame to actual navigation frame, w_{ib}^b the angle rate measured by the gyroscopes in the body frame, f_{ib}^b the specific force measured by the accelerometer in the body frame, w_{ba}^c the rotation velocity of a-frame with respected to b-frame expressed in c-frame. V_E, V_N, V_U are respectively the velocity component in east, north and up direction. L, λ, h denote the latitude, longitude, and height above the earth surface, respectively. R_N is the normal radius. τ_g and τ_f are respectively the correlation time of 1st-order Markovian process for gyroscope and accelerometer. η_g and η_f are the zero-mean Gaussian white noise process.

It should be noted that the bias of the GNSS receiver clock $\delta\mathbf{b}_r$ and its drift $\delta\mathbf{d}_r$ has been modeled and included as state in (52) for the MEMS-SINS/GNSS tightly coupled integrated navigation. They are modeled by random walk as follows:

$$\begin{cases} \delta \dot{\mathbf{b}}_r = \delta \mathbf{d}_r + \mathbf{w}_{br} \\ \delta \dot{\mathbf{d}}_r = \mathbf{w}_{dr} \end{cases} \tag{54}$$

where $\mathbf{w}_{br}$ and $\mathbf{w}_{dr}$ are respectively the white noise for the clock bias and clock drift. The corresponding nonlinear measurement equation of MEMS-SINS/GNSS tightly coupled integrated can be refer to [40] as follows.

$$\mathbf{z}_t = \begin{bmatrix} \delta \mathbf{z}_\rho \\ \delta \mathbf{z}_{\dot{\rho}} \end{bmatrix} = \begin{bmatrix} \rho_{SINS} - \rho_{GNSS} \\ \dot{\rho}_{SINS} - \dot{\rho}_{GNSS} \end{bmatrix} = h\left(\mathbf{x}_k\right) + \boldsymbol{\omega}_{k-1}$$

where ρ_{SINS} and ρ_{GNSS} are respectively the pseudo-range measurement obtained from SINS and GNSS, $\dot{\rho}_{SINS}$ and $\dot{\rho}_{GNSS}$ are respectively the pseudo-range rate obtained from SINS and GNSS. $h\left(\mathbf{x}_k\right)$ can be calculated according to [40].

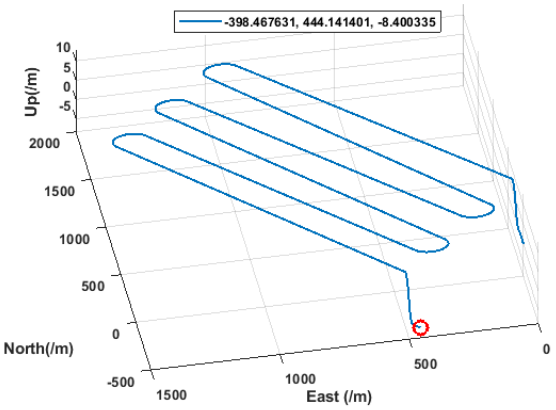

FIGURE 2. True trajectory of the vehicle.

TABLE 1. Description of vehicle motion.

Stage	Period	Maneuver	Parameter
1	0~5.5s	Uniform speed	v=25m/s
2	5.5~5.6s	Turn right at constant angle rate	w=300deg/s
3	5.6~6.6s	Head up at constant angle rate	w=30deg/s
4	6.6~7.6s	Head down at constant angle rate	w=-30deg/s
5	7.6~79.6s	Uniform speed	v=25m/s
6	79.6~88.6s	Turn right at constant angle rate	w=-20deg/s
7	88.6~160.6s	Uniform speed	v=25m/s
8	160.6~169.6s	Turn left at constant angle rate	w=20deg/s
9	169.6~241.6s	Uniform speed	v=25m/s
10	241.6~250.6s	Turn right at constant angle rate	w=-20deg/s
11	250.6~322.6s	Uniform speed	v=25m/s
12	322.6~331.6s	Turn left at constant angle rate	w=20deg/s
13	331.6~403.6s	Uniform speed	v=25m/s
14	403.6~412.6s	Turn right at constant angle rate	w=20deg/s
15	412.6~484.6s	Uniform speed	v=25m/s
16	484.6~485.6s	Head up at constant angle rate	w=30deg/s
17	485.6~486.6s	Head down at constant angle rate	w=30deg/s
18	486.6~488.6s	Uniform speed	v=25m/s

B. SIMULATION RESULT

In order to verify the performance of the proposed RCDKF, the simulation and analysis with different methods are presented based on the tightly coupled MEMS-SINS/GNSS integrated navigation with process uncertainty and non-Gaussian measurement noise. The process model and measurement of tightly coupled MEMS-SINS/GNSS are formulated as

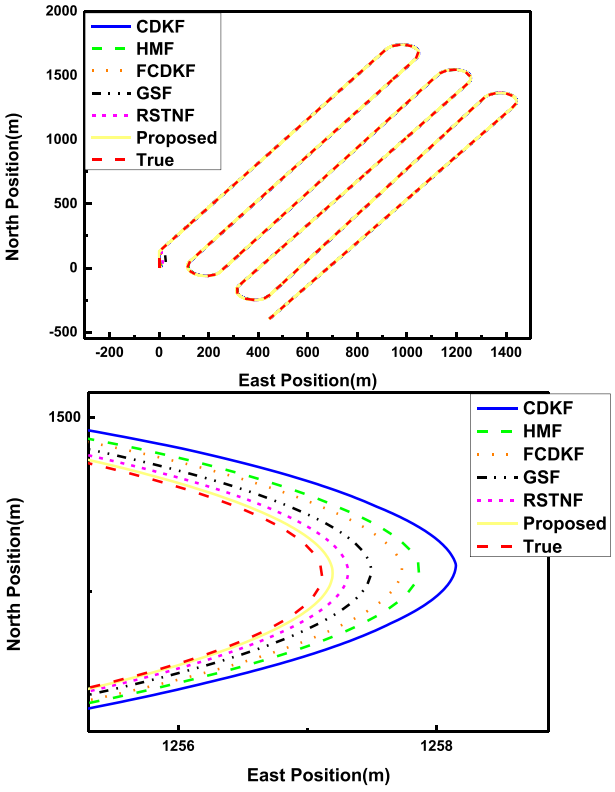

FIGURE 3. True and estimated trajectories of the vehicle.

follows:

$$\begin{aligned} \mathbf{x}_k &= f\left(\mathbf{x}_{k-1}\right) + \mathbf{v}_{k-1} \\ \mathbf{z}_k &= h\left(\mathbf{x}_k\right) + \boldsymbol{\omega}_{k-1} \end{aligned}$$

where $f(\cdot)$ and $h(\cdot)$ are respectively the nonlinear dynamic model function and measurement function. In the tightly coupled MEMS-SINS/GNSS, $f(\cdot)$ can be obtained from equation (53)-(54) and the observation vector is obtained according to [40]. $\mathbf{v}_{k-1}$ and $\boldsymbol{\omega}_{k-1}$ are respectively the zero mean non-Gaussian process and measurement noise, and the process uncertainty and non-Gaussian measurement noise are generated according to [23]:

$$\mathbf{v}_k \sim \begin{cases} N\left(\mathbf{0}, \mathbf{Q}_k\right), & w.p.\ 0.8 \\ N\left(\mathbf{0}, 100\mathbf{Q}_k\right), & w.p.\ 0.2 \end{cases} \tag{55}$$

$$\mathbf{w}_k \sim \begin{cases} N\left(\mathbf{0}, \mathbf{R}_k\right), & w.p.\ 0.8 \\ N\left(\mathbf{0}, 100\mathbf{R}_k\right), & w.p.\ 0.2 \end{cases} \tag{56}$$

where $N(\boldsymbol{\mu}, \boldsymbol{\Sigma})$ denotes the Gaussian distribution with mean $\boldsymbol{\mu}$ and covariance matrix $\boldsymbol{\Sigma}$, $\mathbf{Q}_k$ and $\mathbf{R}_k$ are the nominal covariance matrixes from the Gaussian distribution, Equation (55) and (56) imply that $\mathbf{v}_k$ and $\mathbf{w}_k$ are most frequently drawn from a Gaussian distribution with nominal covariance matrix $\mathbf{Q}_k$ and $\mathbf{R}_k$, and twenty percent of process and measurement noise are generated from the Gaussian distribution with severely increased covariance.

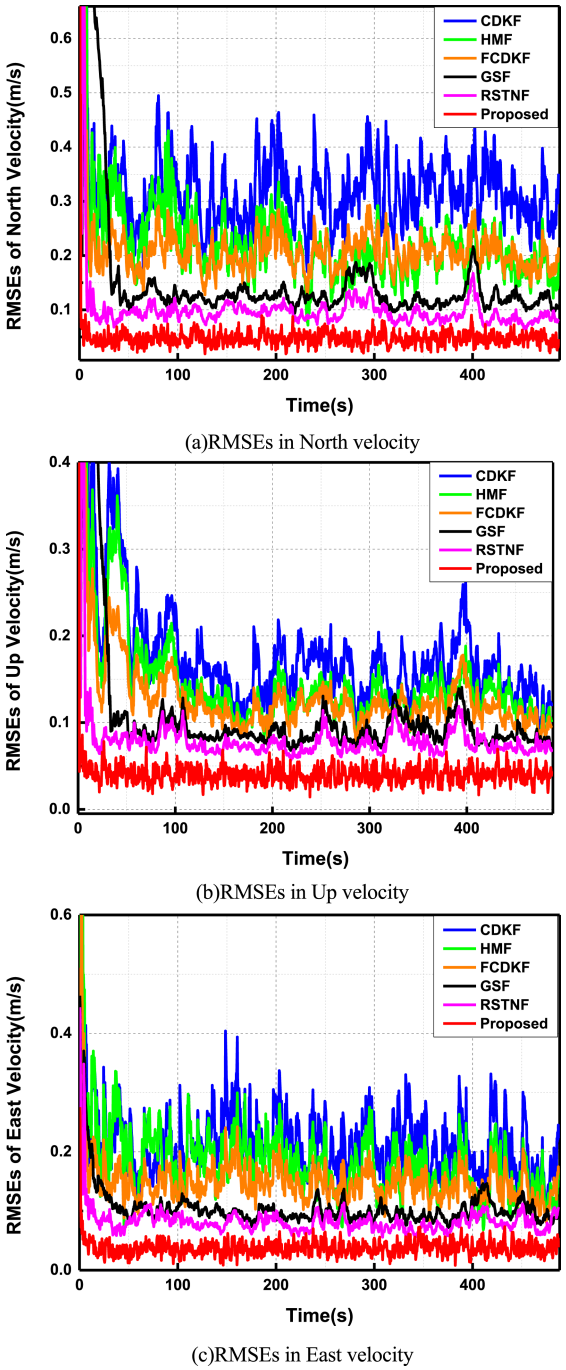

(a)RMSEs in North velocity

(b)RMSEs in Up velocity

(c)RMSEs in East velocity

FIGURE 4. Estimated velocity RMSEs of different filters.

In our simulation, the vehicle has done a series of maneuvers according to Table 1. The total simulation time is 488.6s. The true trajectory of the vehicle is shown in Figure 2.

The update frequency of GNSS and MEMS-SINS are respectively 10Hz and 1KHz. The constant drift of gyroscope and accelerometer are respectively 12deg/h and 10mg. The random drift of gyroscope and accelerometer are respectively 0.3deg/sqrt(h) and 0.3m/s^2/sqrt(Hz). The initial position is $\mathbf{PosN0} = \left[38.014^\circ\ 836m\ 112.445^\circ\right]^T$, initial velocity is $\mathbf{VelN0} = \left[25m/s\ 0\ 0\right]^T$ and initial

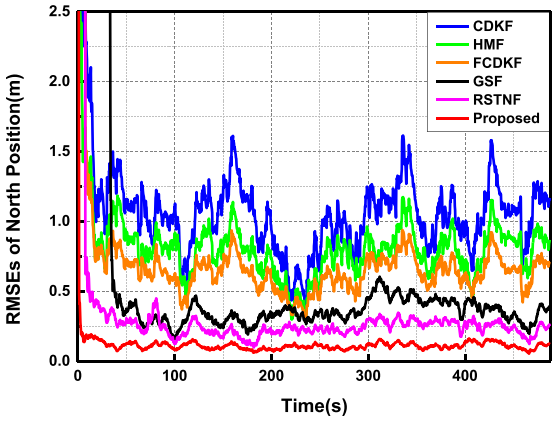

(a)RMSEs in North Position

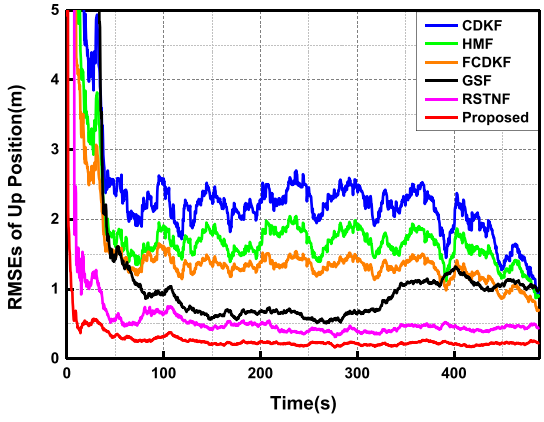

(b)RMSEs in Up Position

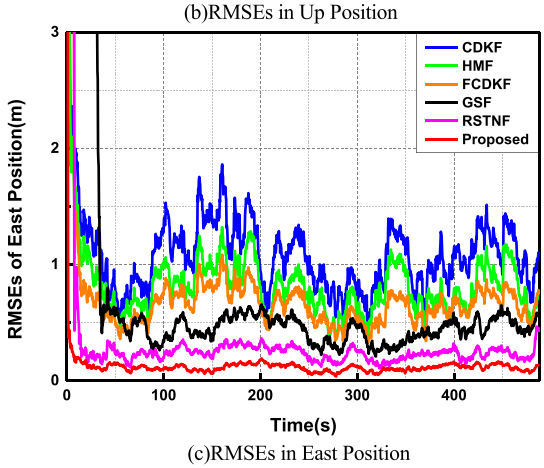

(c)RMSEs in East Position

FIGURE 5. Estimated position RMSEs of different filters.

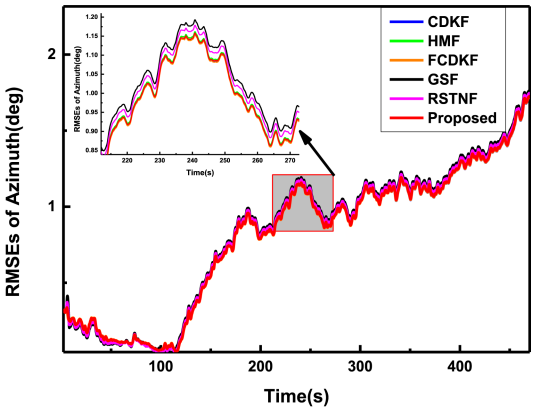

(a)RMSEs of Azimuth

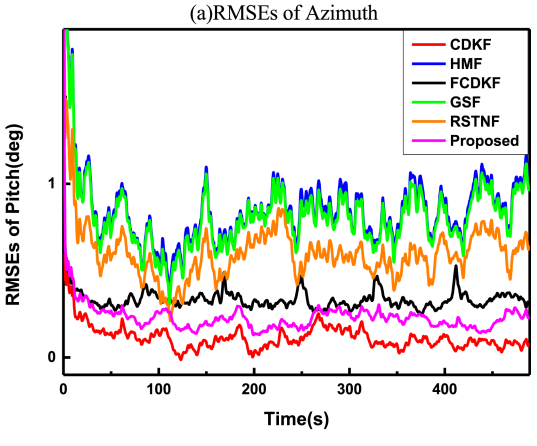

(b)RMSEs of Pitch

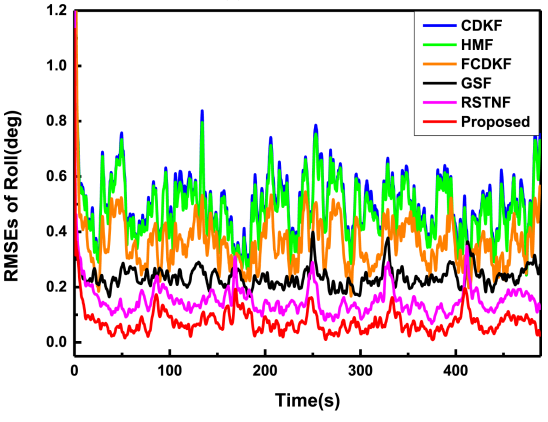

(c)RMSEs of Roll

FIGURE 6. Estimated attitude RMSEs of different filters.

attitude is $\mathbf{q0} = [1\ 0\ 0\ 0]^T$. The constant drift of gyroscope and accelerometer are respectively set as $\varepsilon_b = \left[12^\circ/h\ 12^\circ/h\ 12^\circ/h\right]^T$, $\nabla_b = \left[10mg\ 10mg\ 10mg\right]^T$.

In this simulation, the initial state vector and the associated covariance are set as $\hat{\mathbf{x}}_{0|0} = 0_{23\times1}$ and $\mathbf{P}_{0|0} = \text{diag}([0.005\text{rad}, 0.015\text{rad}, 0.005\text{rad}, 0.1\text{m/s}, 0.1\text{m/s}, 0.1\text{m/s}, 1\text{m}, 3\text{m}, 1\text{m}, 0.2\text{deg/s}, 0.2\text{deg/s}, 0.2\text{deg/s}, 16\text{mg}, 16\text{mg}, 16\text{mg}, 0.0018\text{deg/s}, 0.0018\text{deg/s}, 0.0018\text{deg/s}, 0.1\text{mg}, 0.1\text{mg}, 0.1\text{mg}, 10\text{m}, 0.1\text{m/s}])^2$, respectively. The initial value of the nominal process noise covariance matrix and measurement noise covariance matrix are respectively set as $\mathbf{Q}_k = \text{diag}([0.3\text{deg/sqrt(h)}, 0.3\text{deg/sqrt(h)}, 0.3\text{deg/sqrt(h)}, 0.3\text{m/s}^2\text{/sqrt(Hz)}, 0.3\text{m/s}^2\text{/sqrt(Hz)}, 0.3\text{m/s}^2\text{/sqrt(Hz)}, 0.3\text{deg/sqrt(h)}, 0.3\text{deg/sqrt(h)}, 0.3\text{deg/sqrt(h)}, 0.3\text{m/s}^2\text{/sqrt(Hz)}, 0.3\ \text{m/s}^2\text{/sqrt(Hz)}, 0.3\text{m/s}^2\text{/sqrt(Hz)}], 1\text{m/s}, 1\text{m/s}^2)^2$ and $\mathbf{R}_k = [\mathbf{I}_{\text{M}\times\text{M}}{}^*(2.5\text{m})^2\mathbf{0}_{\text{M}\times\text{M}}; \mathbf{0}_{\text{M}\times\text{M}}\mathbf{I}_{\text{M}\times\text{M}}{}^*(1\text{m/s}^2)^2]$(M is the number of visible satellite). To validate the superiority of our proposed RCDKF, the performance of the following methods is compared, including the existing central difference Kalman fitler (CDKF)[41], fading central difference Kalman filter(FCDKF), Huber's M-estimation filter(HMF) [20], robust Student's t based nonlinear filter

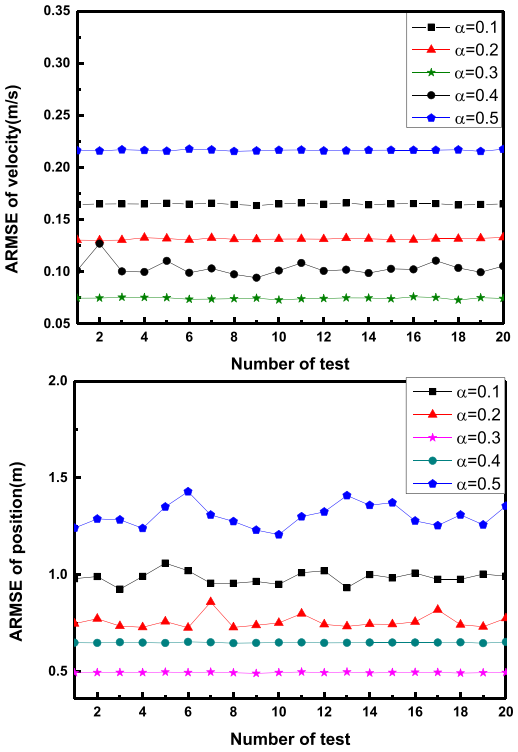

FIGURE 7. ARMSEs of the three-dimension velocity and position.

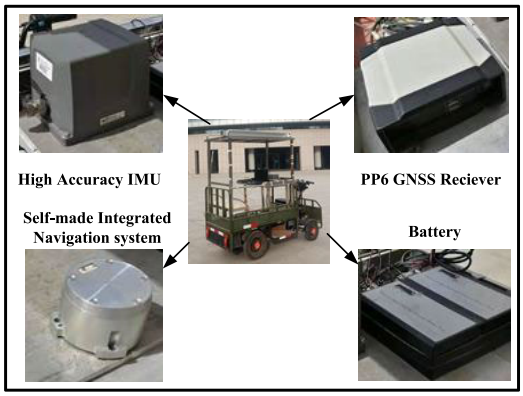

FIGURE 8. The car-mounted experimental platform used in this experiment.

(RSTNF) [24] and Gaussian sum filter(GSF) [42]. In the HMF, the turning parameter is set as: $\gamma = 1.5, N = 10$. In the RSTNF, the dof parameter, turning parameter and the iteration number are chosen as: $\nu = 5$, $\tau = 5$ and $N = 10$. The filtering algorithms are all coded with MATLAB and the simulations are run on a computer with intel core i5-3320 CPU at 2.60GHz, 4Gb memory.

To compare the filtering performance of the proposed methods and existing methods, the RMSEs and the averaged RMSEs (ARMSE) of attitude, velocity and position with respect to time for the MEMS-SINS/GNSS integrated navigation system are chosen as performance metrics in this

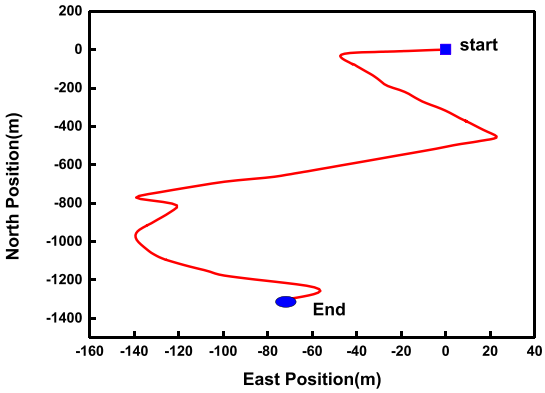

FIGURE 9. The test trajectory in the car-mounted experiment.

simulation, which are respectively formulated as

$$RMSE = \sqrt{\frac{1}{M}\sum_{s=1}^{M}\left(x_k^s - \hat{x}_k^s\right)^2} \tag{57}$$

$$ARMSE = \sqrt{\frac{1}{MT}\sum_{k=1}^{T}\sum_{s=1}^{M}\left(x_k^s - \hat{x}_k^s\right)^2} \tag{58}$$

where x_k^s and $\hat{x}_k^s$ denote the true and the estimated value of attitude, velocity and position at time k of the sth Monte Carlo run, respectively. M denotes the number of Monte Carlo run. T represents the total simulation samples.

In the tightly-couple MEMS-SINS/GNSS integrated navigation, the true and estimated trajectories of the vehicle obtained from the five algorithms in a single step run are shown in Figure 3. The RMSEs of velocity, position and attitude obtained from the five existing filters and the proposed filter are shown in Figure 4-6. It is clear from Figure 3 that the trajectory computed by the proposed robust central difference Kalman filter is more consistent with the real trajectory compared with the other five algorithms. It can be also seen that that the proposed filter has smaller RMSEs of velocity and position than the existing CDKF, FCDKF, HMF, RSTNF and GSF, which indicates that the proposed method has a higher navigation position accuracy under the condition of process uncertainty and non-Gaussian. Meanwhile, the implementation time of the CDKF, FCDKF, HMF, RSTNF, GSF and the proposed filter for a single step run are respectively 0.432ms, 0.456ms, 0.439ms, 0.468ms, 0.735 and 0.452ms, which proves that the proposed method under the traditional Kalman filter framework has a better computational efficiency. Therefore, taking both the estimation accuracy and computational efficiency into account, we can conclude that the proposed RCDKF can achieve better performance with the compromised computational cost when compared with the existing state-of-art methods.

The mixture coefficient of mix-correntropy may affect the performance of our proposed RCDKF, so the simulations with different mixture coefficient were conducted. The mixture coefficient varies from 0 to 0.5, and the interval of the increased step is 0.1. The corresponding ARMSE of the

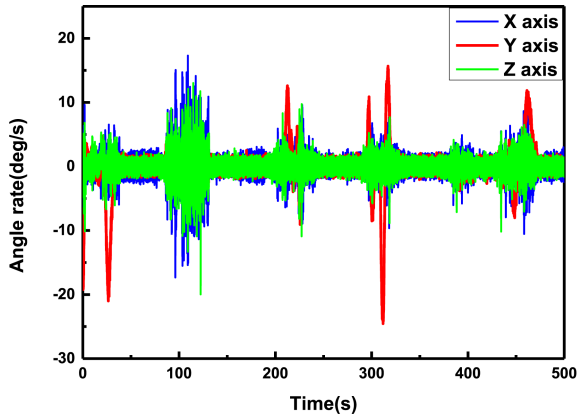

(a)The raw output of 3-D gyroscopes

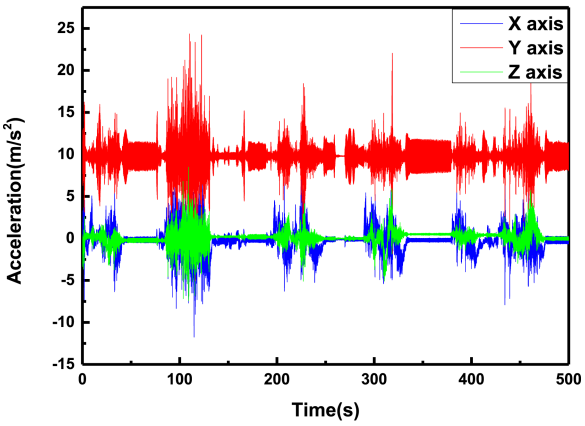

(b)The raw output of 3-D accelerometer

FIGURE 10. The raw output of IMU.

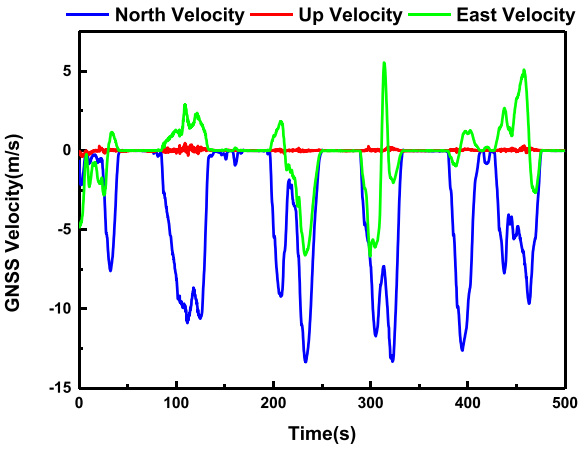

FIGURE 11. The velocity output of GNSS.

three-dimension velocity, position and attitude are respectively displayed in Figure 7. From the figures, we can see that a good performance can be achieved when the mixture coefficient is selected as $\alpha = 0.3$.

C. CAR-MOUNTED FIELD TEST FOR TIGHTLY COUPLED MEMS-SINS/GNSS INTEGRATION NAVIGATION

1) EXPERIMENT SETUP AND DESCRIPTION

To verify the effectiveness of the proposed RCDKF, a car-mounted field test using our self-made miniature

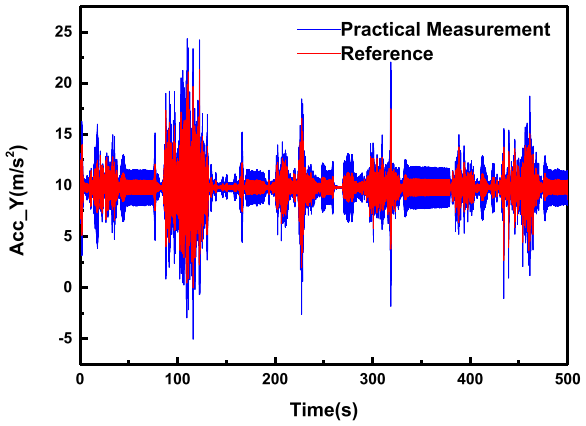

FIGURE 12. The practical and reference measurement of Y-axis accelerometer in the experiment.

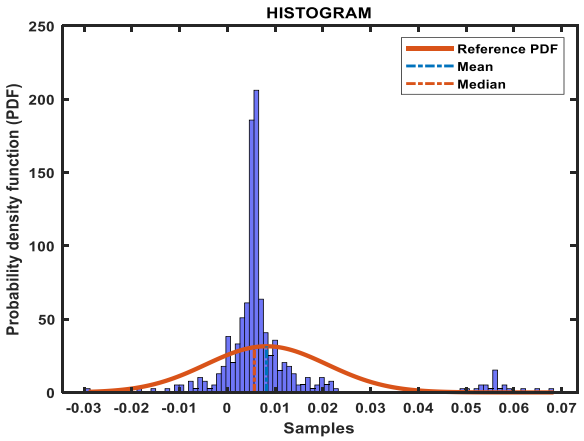

(a) The statistical curve of north velocity error

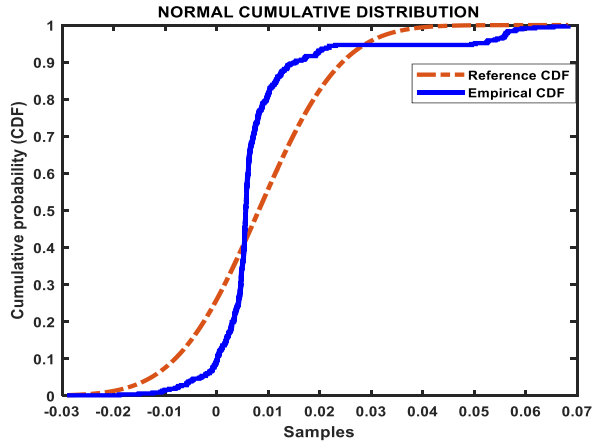

(b)The cumulative distribution of north velocity error

FIGURE 13. The distribution of north velocity error.

MEMS-SINS/GNSS integration navigation system was conducted. In the experimental test, a high precision car-mounted experimental platform consisting of a LCI-1 tactical grade IMU (inertial measurement unite), a Propak satellite receiver, and two GPS antennas is constructed as shown in Figure 8. The benchmark of attitude, velocity and position for our

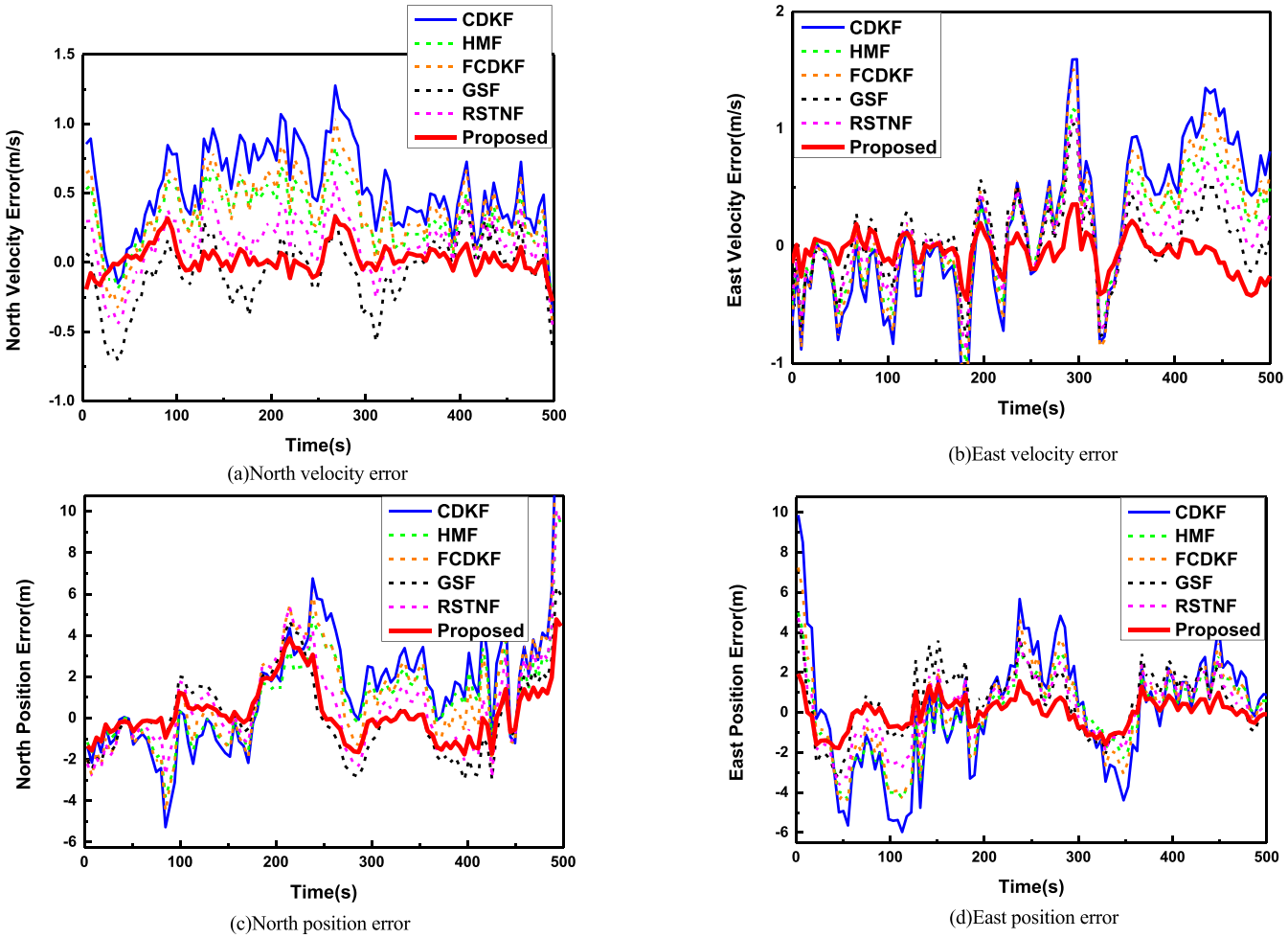

(a)North velocity error

(b)East velocity error

(c)North position error

(d)East position error

FIGURE 14. Velocity error and position error from different filters.

self-made MEMS-SINS/GNSS integration navigation system is provided by the car-mounted experimental platform. For the car-mounted experimental platform, the attitude accuracy is 0.01°, the velocity accuracy is 0.05m/s and the position accuracy is 0.1m. The sensors specification of our self-made MEMS-SINS/GNSS integration navigation system is listed in Table 2. The experiment lasted for a period of approximately 500s. The test trajectory is shown in Figure 9. In the experimental test, the car moves along a dump road and the GPS always works abnormally due to the occlusion of trees and buildings. The raw output of IMU and velocity output of GNSS are respectively displayed in Figure 10 and Figure 11. The practical and reference measurement of Y-axis accelerometer and the distribution of north velocity error in the experiment are respectively shown in Figure 12 and Figure 13. It can be clearly seen from Figure 12-13 that the process noise exist notable uncertainty and the measurement noise has heavy-tails, which cannot satisfy the Gaussian distribution. Therefore, we use the car-mounted experiment under this condition to verify the performance of the proposed filter against process uncertainty and non-Gaussian measurement noise.

TABLE 2. Sensors specifications of our self-made MEMS-SINS/GNSS integration navigation system.

Quantity	Gyroscope	Accelerometer
Range	$\pm 400^\circ$ /s	± 5g
Bias	10° /h	0.5mg
Random walk	$0.28\,\mathrm{deg}/\sqrt{h}$	$90\,\mathrm{ug}/\sqrt{Hz}$

2) PERFORMANCE COMPARISON WITH DIFFERENT ROBUST FILTERING ALGORITHMS

In this section, the proposed RCDKF is compared with the central difference Kalman fitler (CDKF)[41], fading central difference Kalman filter(FCDKF), Huber's M-estimation filter(HMF) [20], robust Student's t based nonlinear filter (RSTNF) [24] and Gaussian sum filter(GSF)[42] in the car-mounted experiment to evaluate the overall performance for MEMS-SINS/GNSS integration navigation system. The parameter configuration of the proposed filter and existing filters are set as follows: In the HMF, the turning parameter is set as: $\gamma = 1.5, N = 10$. In the RSTNF, the dof parameter, turning parameter and the iteration number are chosen as: $v = 0.2$, $\tau = 5$ and $N = 5$. In our proposed robust central

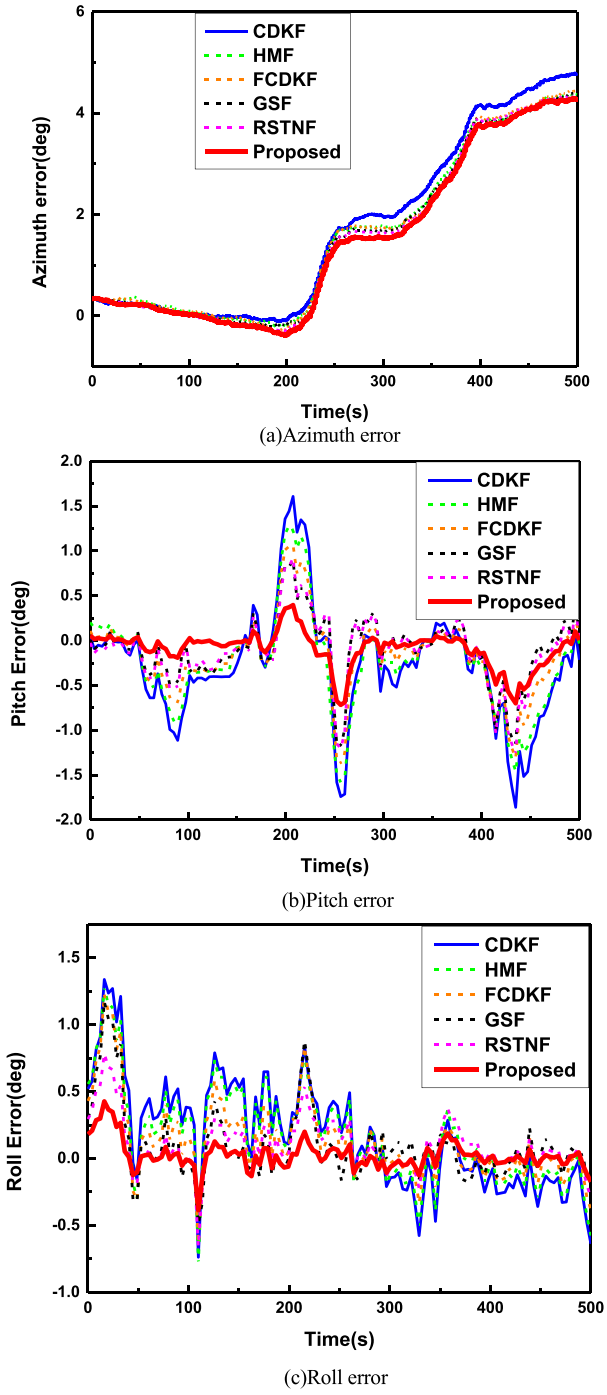

FIGURE 15. Attitude error from different filters.

difference Kalman filter, the mixture coefficient and kernel size are respectively set as: $\alpha = 0.3$, $\sigma_1 = 10$ and $\sigma_2 = 10$. The other parameters are the same as those in the simulation part.

The velocity, position and attitude error results obtained from the different algorithms are shown in Figure 14-15, and the corresponding RMSEs are listed in Table 3. We can clearly see that the performance of the existing five robust filters is superior to their non-robust counterpart (CDKF).This is because that the fusion algorithm based on traditional

TABLE 3. RMSEs of velocity and position from different algorithms.

Filters	RMSE					
	PosN (m)	PosE (m)	VelN (m/s)	VelE (m/s)	Pitch (deg)	Roll (deg)
CDKF	3.262	2.894	0.615	0.651	0.543	0.403
HMF	3.002	2.225	0.491	0.567	0.443	0.362
FCDKF	2.363	1.911	0.463	0.452	0.382	0.301
GSF	2.310	1.648	0.246	0.373	0.370	0.276
RSTNF	1.945	1.634	0.241	0.328	0.306	0.202
Proposed	1.417	0.767	0.105	0.168	0.203	0.106

Gaussian filtering are not suitable for the nonlinear system with uncertain noise. It is notable that HMF outperforms CDKF, which indicates that Huber's M-estimation is effective for the non-Gaussian measurement noise. Meanwhile, the FCDKF with the multiple-channel adaptive fading factor exist smaller velocity and position RMSE than CDKF but large velocity and position RMSE than the proposed RCDKF, which demonstrates that the proposed RCDKF with only the fading factor can effectively deal with the time-varing process noise. In contrast, the GSF and RSTNF using the multiple-model and student's t method can better suppress both of the process uncertainty and non-Gaussian measurement noise, and can achieve better performance than HMF and FCDKF. We can also see that our proposed RCDKF is superior to GSF and RSTNF, which coincides with the fact that our proposed adaptive mixture correntropy technology is more effective than the multiple-model filtering and student's t-based Kalman filtering technology. Therefore, the experimental results indicate that the proposed robust central difference Kalman filter can simultaneously handle the process uncertainty and non-Gaussian measurement noise and achieve better performance than the existing robust filters under the condition of vehicle's severe maneuver and abnormal measurements in MEMS-SINS/GNSS integrated navigation system.

V. CONCLUSION

In this paper, a new robust central difference Kalman filter for the MEMS-SINS/GNSS integration navigation system is proposed, which exhibit strong robustness against the process uncertainty and measurement noise induced by the vehicle's severe maneuver and abnormal measurements of the velocity and position from GNSS. In the proposed robust central difference Kalman filter, the statistical linearization method is firstly used to convert the traditional nonlinear central difference Kalman filter into an equivalent linear-like regression form. Then, the criteria for bounding the state estimation error caused by process uncertainty and non-Gaussian noise is constructed. Subsequently, a new robust central difference Kalman filter based on the proposed criteria is formulated. Moreover, an adaptive strategy is proposed to automatically tune the fading factor responding to the changeable condition. Simulations and car-mounted experiments indicate that the proposed new robust central difference Kalman filter can

achieve high estimation accuracy and better robustness than the existing state-of-art methods against the process uncertainty and non-Gaussian measurement noise.

REFERENCES

[1] J. Farrell, *Aided Navigation: GPS With High Rate Sensors*. New York, NY, USA: McGraw-Hill, 2008.
[2] J. Farrell and M. Barth, *The Global Positioning System and Inertial Navigation*, vol. 61. New York, NY, USA: McGraw-Hill, 1999.
[3] P. D. Groves, *Principles of GNSS, Inertial, and Multisensor Integrated Navigation Systems*. Norwood, MA, USA: Artech House, 2013.
[4] C. Shen, Y. Zhang, X. Guo, X. Chen, H. Cao, J. Tang, J. Li, and J. Liu, "Seamless GPS/inertial navigation system based on self-learning square-root cubature Kalman filter," *IEEE Trans. Ind. Electron.*, vol. 68, no. 1, pp. 499–508, Jan. 2021.
[5] G. Hu, W. Wang, Y. Zhong, B. Gao, and C. Gu, "A new direct filtering approach to INS/GNSS integration," *Aerosp. Sci. Technol.*, vol. 77, pp. 755–764, Jun. 2018.
[6] G. Hu, S. Gao, and Y. Zhong, "A derivative UKF for tightly coupled INS/GPS integrated navigation," *ISA Trans.*, vol. 56, pp. 135–144, May 2015.
[7] D. Simon, *Optimal State Estimation: Kalman, H Infinity, and Nonlinear Approaches*. Hoboken, NJ, USA: Wiley, 2006.
[8] Q. Zhang, X. Meng, S. Zhang, and Y. Wang, "Singular value decomposition-based robust cubature Kalman filtering for an integrated GPS/SINS navigation system," *J. Navigat.*, vol. 68, no. 3, pp. 549–562, May 2015.
[9] Y. Huang and Y. Zhang, "A new process uncertainty robust Student's t based Kalman filter for SINS/GPS integration," *IEEE Access*, vol. 5, pp. 14391–14404, 2017.
[10] M. Liu, J. Lai, Z. Li, and J. Liu, "An adaptive cubature Kalman filter algorithm for inertial and land-based navigation system," *Aerosp. Sci. Technol.*, vol. 51, pp. 52–60, Apr. 2016.
[11] M. Zhong, J. Guo, and Q. Cao, "On designing PMI Kalman filter for INS/GPS integrated systems with unknown sensor errors," *IEEE Sensors J.*, vol. 15, no. 1, pp. 535–544, Jan. 2015.
[12] M. Karasalo and X. Hu, "An optimization approach to adaptive Kalman filtering," *Automatica*, vol. 47, no. 8, pp. 1785–1793, Aug. 2011.
[13] R. Mehra, "Approaches to adaptive filtering," *IEEE Trans. Autom. Control*, vol. AC-17, no. 5, pp. 693–698, Oct. 1972.
[14] C. Hide, T. Moore, and M. Smith, "Adaptive Kalman filtering for low-cost INS/GPS," *J. Navigat.*, vol. 56, no. 1, pp. 143–152, Jan. 2003.
[15] I. Bilik and J. Tabrikian, "MMSE-based filtering in presence of non-Gaussian system and measurement noise," *IEEE Trans. Aerosp. Electron. Syst.*, vol. 46, no. 3, pp. 1153–1170, Jul. 2010.
[16] D. H. Zhou and P. M. Frank, "Strong tracking filtering of nonlinear time-varying stochastic systems with coloured noise: Application to parameter estimation and empirical robustness analysis," *Int. J. Control*, vol. 65, no. 2, pp. 295–307, Sep. 1996.
[17] K. Feng, J. Li, X. Zhang, X. Zhang, C. Shen, H. Cao, Y. Yang, and J. Liu, "An improved strong tracking cubature Kalman filter for GPS/INS integrated navigation systems," *Sensors*, vol. 18, no. 6, p. 1919, Jun. 2018.
[18] G. Hu, S. Gao, Y. Zhong, B. Gao, and A. Subic, "Modified strong tracking unscented Kalman filter for nonlinear state estimation with process model uncertainty," *Int. J. Adapt. Control Signal Process.*, vol. 29, no. 12, pp. 1561–1577, Dec. 2015.
[19] P. J. Huber, *Robust Statistics*. Hoboken, NJ, USA: Wiley, 2004.
[20] L. Chang, K. Li, and B. Hu, "Huber's M-estimation-based process uncertainty robust filter for integrated INS/GPS," *IEEE Sensors J.*, vol. 15, no. 6, pp. 3367–3374, Jun. 2015.
[21] G. Chang and M. Liu, "M-estimator-based robust Kalman filter for systems with process modeling errors and rank deficient measurement models," *Nonlinear Dyn.*, vol. 80, no. 3, pp. 1431–1449, May 2015.
[22] L. Chang, B. Hu, G. Chang, and A. Li, "Robust derivative-free Kalman filter based on Huber's M-estimation methodology," *J. Process Control*, vol. 23, no. 10, pp. 1555–1561, Nov. 2013.
[23] Y. Huang and Y. Zhang, "Robust Student's t-based stochastic cubature filter for nonlinear systems with heavy-tailed process and measurement noises," *IEEE Access*, vol. 5, pp. 7964–7974, 2017.
[24] Y. Huang, Y. Zhang, N. Li, and J. Chambers, "Robust Student's t based nonlinear filter and smoother," *IEEE Trans. Aerosp. Electron. Syst.*, vol. 52, no. 5, pp. 2586–2596, Oct. 2016.
[25] Y. Huang, Y. Zhang, N. Li, Z. Wu, and J. A. Chambers, "A novel robust Student's t-based Kalman filter," *IEEE Trans. Aerosp. Electron. Syst.*, vol. 53, no. 3, pp. 1545–1554, Jan. 2017.
[26] Y. Huang, Y. Zhang, B. Xu, Z. Wu, and J. Chambers, "A new outlier-robust Student's t based Gaussian approximate filter for cooperative localization," *IEEE/ASME Trans. Mechatronics*, vol. 22, no. 5, pp. 2380–2386, Oct. 2017.
[27] Z. Zhu, Z. Meng, Z. Zhang, J. Chen, and Y. Dai, "Robust particle filter for state estimation using measurements with different types of gross errors," *ISA Trans.*, vol. 69, pp. 281–295, Jul. 2017.
[28] M. Corbetta, C. Sbarufatti, M. Giglio, and M. D. Todd, "Optimization of nonlinear, non-Gaussian Bayesian filtering for diagnosis and prognosis of monotonic degradation processes," *Mech. Syst. Signal Process.*, vol. 104, pp. 305–322, May 2018.
[29] W. Li, Z. Wang, Y. Yuan, and L. Guo, "Two-stage particle filtering for non-Gaussian state estimation with fading measurements," *Automatica*, vol. 115, May 2020, Art. no. 108882.
[30] J. Lim, "Particle filtering for nonlinear dynamic state systems with unknown noise statistics," *Nonlinear Dyn.*, vol. 78, no. 2, pp. 1369–1388, Oct. 2014.
[31] L. Úbeda-Medina, Á. F. García-Fernández, and J. Grajal, "Sigma-point multiple particle filtering," *Signal Process.*, vol. 160, pp. 271–283, Jul. 2019.
[32] K. Feng, J. Li, D. Zhang, X. Wei, and J. Yin, "Robust cubature Kalman filter for SINS/GPS integrated navigation systems with unknown noise statistics," *IEEE Access*, vol. 9, pp. 9101–9116, 2021.
[33] K. Feng, J. Li, D. Zhang, X. Wei, and J. Yin, "AGMC-based robust cubature Kalman filter for SINS/GNSS integrated navigation system with unknown noise statistics," *IEEE Access*, vol. 9, pp. 1693–1706, 2021.
[34] W. Liu, P. P. Pokharel, and J. C. Principe, "Correntropy: Properties and applications in non-Gaussian signal processing," *IEEE Trans. Signal Process.*, vol. 55, no. 11, pp. 5286–5298, Nov. 2007.
[35] B. Chen and J. C. Principe, "Maximum correntropy estimation is a smoothed MAP estimation," *IEEE Signal Process. Lett.*, vol. 19, no. 8, pp. 491–494, Aug. 2012.
[36] J. C. Principe, *Information Theoretic Learning: Renyi's Entropy and Kernel Perspectives*. Springer, 2010.
[37] R. Izanloo, S. A. Fakoorian, H. S. Yazdi, and D. Simon, "Kalman filtering based on the maximum correntropy criterion in the presence of non-Gaussian noise," in *Proc. IEEE Annu. Conf. Inf. Sci. Syst. (CISS)*, Mar. 2016, pp. 500–505.
[38] B. Chen, X. Liu, H. Zhao, and J. C. Principe, "Maximum correntropy Kalman filter," *Automatica*, vol. 76, pp. 70–77, Feb. 2017.
[39] G. T. Cinar and J. C. Príncipe, "Hidden state estimation using the correntropy filter with fixed point update and adaptive kernel size," in *Proc. Int. Joint Conf. Neural Netw. (IJCNN)*, 2012, pp. 1–6.
[40] A. Noureldin, T. B. Karamat, and J. Georgy, *Fundamentals of Inertial Navigation, Satellite-Based Positioning and Their Integration*. Springer, 2012.
[41] P. Stano, Z. Lendek, J. Braaksma, R. Babuska, C. de Keizer, and A. J. den Dekker, "Parametric Bayesian filters for nonlinear stochastic dynamical systems: A survey," *IEEE Trans. Cybern.*, vol. 43, no. 6, pp. 1607–1624, Dec. 2013.
[42] D. Alspach and H. Sorenson, "Nonlinear Bayesian estimation using Gaussian sum approximations," *IEEE Trans. Autom. Control*, vol. AC-17, no. 4, pp. 439–448, Aug. 1972.

KAIQIANG FENG received the B.S. and Ph.D. degrees from the Department of Instrument and Electronics, North University of China, Taiyuan, China, in 2015 and 2019, respectively, where he is currently pursuing the Ph.D. degree in armament science and technology. His current research interests include inertial navigation, inertial-based integrated navigation systems, and state estimation theory.

JIE LI was born in Lvliang, Shanxi, China, in 1976. He received the Ph.D. degree from the Department of Automation, Beijing University of Technology, Beijing, China, in 2005. He is currently a Professor of navigation, guidance and control with the North University of China, China. His current research interests include inertial sensing and control, inertial-based integrated navigation theory, and microsystem integration.

DEBIAO ZHANG was born in Jiaxiang, Shandong, China, in June 1989. He is currently pursuing the Ph.D. degree in instrument science and technology with the School of Instrument and Electronics, North University of China. He is currently engaged in research on inertial navigation.

XIAOKAI WEI was born in Nei Mongol, China, in 1992. He received the B.E. degree in weapon system and launch engineering from the College of Mechatronic Engineering, North University of China, Taiyuan, China, in 2015, where he is currently pursuing the Ph.D. degree in instrument science and technology. His current research interests include inertial navigation, integrated navigation, and adaptive control.

JIANPING YIN was born in Yuxian, Shanxi, China, in 1975. He received the Ph.D. degree from the College of Mechatronic Engineering, North University of China, China, in 2010. He is currently a Professor of armament science and technology with the North University of China. His current research interests include munitions damage technology and munitions guidance technology.